Enhanced dissolution of silver nanoparticles in a physical mixture with platinum nanoparticles based on the sacrificial anode effect

Marina Breisch[1*], Kateryna Loza[2], Kevin Pappert[2], Alexander Rostek[2], Christian Rurainsky[3], Kristina Tschulik[3], Marc Heggen[4], Matthias Epple[2], Jörg C. Tiller[5], Thomas A. Schildhauer[1], Manfred Köller[1], Christina Sengstock[1]

[1] BG University Hospital Bergmannsheil Bochum / Surgical Research, Ruhr University Bochum, Buerkle-de-la-Camp-Platz 1, D-44789 Bochum, Germany. Fax: +49 234 3024734; Tel: +49 234 3024724; E-mail: marina.breisch@tu-dortmund.de

[2] University of Duisburg-Essen, Inorganic Chemistry and Center for Nanointegration Duisburg-Essen (CeNIDE), Universitaetsstr. 5-7, D-45117 Essen, Germany.

[3] Ruhr University Bochum, Faculty of Chemistry and Biochemistry, Electrochemistry and Nanoscale Materials, Universitätsstr. 150, D-44780 Bochum, Germany.

[4] Ernst Ruska-Centre (ER-C) for Microscopy and Spectroscopy with Electrons, Research Center Jülich GmbH, 52425 Jülich, Germany.

[5] TU Dortmund University, Faculty of Biochemical and Chemical Engineering, Institute for Biomaterials and Polymer Science, Emil-Figge-Straße 50, 44227 Dortmund, Germany.

***** Corresponding author, Tel: +49 234 3024724, Fax: +49 234 3024734, e-mail: marina.breisch@tu-dortmund.de

Abstract

A strategy to reduce implant-related infections is the inhibition of the initial bacterial implant colonization by biomaterials containing silver (Ag). The antimicrobial efficacy of such biomaterials can be increased by surface enhancement (nanosilver) or by creating a sacrificial anode system for Ag. Such a system will lead to an electrochemically driven enhanced Ag ion release due to the presence of a more noble metal. Here we combined the enlarged surface of nanoparticles (NP) with a possible sacrificial anode effect for Ag induced by the presence of the electrochemically more noble platinum (Pt) in physical mixtures of Ag NP and Pt NP dispersions.

These Ag NP / Pt NP mixtures were compared to same amounts of pure Ag NP in terms of cell biological responses, i.e. the antimicrobial activity against *Staphylococcus aureus* and *Escherichia coli* as well as the viability of human mesenchymal stem cells (hMSC). In addition, Ag NP was analyzed by ultraviolet–visible (UV-Vis) spectroscopy, cyclic voltammetry (CV), and atomic absorption spectroscopy (AAS).

It was found that the dissolution rate of Ag NP was enhanced in the presence of Pt NP within the physical mixture compared to a dispersion of pure Ag NP. Dissolution experiments revealed a fourfold increased Ag ion release from physical mixtures due to enhanced electrochemical activity, which resulted in a significantly increased toxicity towards both bacteria and hMSC. Thus, our results provide evidence for an underlying sacrificial anode mechanism induced by the presence of Pt NP within physical mixtures with Ag NP. Such physical mixtures have a high potential for various applications, for example as antimicrobial implant coatings in the biomedicine or as bactericidal systems for water and surface purification in the technical area.

Keywords: sacrificial anode, antimicrobial activity, silver nanoparticles, platinum nanoparticles, physical mixture

1. Introduction

Despite best clinical practice, implant-related infections remain a serious clinical problem [1]. Antimicrobially active biomaterials or coatings containing silver (Ag) which could prevent or hinder the initial bacterial adhesion, colonization and biofilm formation are promising approaches to reduce implant-related infections.

Numerous studies demonstrated the capability of Ag to reduce infections and bacterial colonization of burn dressings, catheters, dental implants and other medical devices [2–6]. It is now generally accepted that the biological action of Ag is based on the oxidative release of silver ions (Ag^+) which interact with various biomolecules such as enzymes, nucleic acids and cell wall components [7–10]. Thus, the antibacterial activity of Ag is governed by the amount of released Ag^+. In general, the increased surface area of Ag nanoparticles (NP) compared to macroscale Ag leads to a more efficient Ag^+ release [11].

In previous studies we investigated an alternative approach to enhance the Ag^+ release by the combination of Ag with an electrochemically more noble metal, i.e. a platinum group element, based on the sacrificial anode principle [12–14]. Generally, when two electrochemically different metals are present in an electrolytic environment, an anodic polarization is induced, and the less noble metal is dissolved ("sacrificed") in favor of the more noble one by corrosion [15]. Sacrificial anodes are widespread in the technical area [15–17], but have not received much attention in biomedical applications so far.

There are only few studies that have addressed the biological effects of Ag-related sacrificial anode-like systems. Zhang *et al.* found that bimetallic nanosheets of Ag (7 nm) and platinum (Pt; 1 – 3 nm) on porous reduced graphene oxide showed increased antimicrobial activity against *Escherichia coli* due to an enhanced Ag^+ release compared to pure Ag sheets [18]. Dowling *et al.* demonstrated an improved antibacterial efficiency of alloyed bimetallic AgPt coatings on polymeric surfaces compared to pure Ag coatings [19]. Our group showed the efficiency of sacrificial anode systems consisting of Ag dots deposited on thin metal films of gold, platinum, palladium or iridium [12–14].

Recently, we investigated whether an enhanced Ag^+ release based on the sacrificial anode principle could be achieved by combination of Ag with the electrochemically more noble Pt in the form of NP. We found that no sacrificial anode effect was

induced in bimetallic alloyed AgPt NP [20,21]. Therefore, we investigated mixtures of non-alloyed Ag NP and Pt NP (physical mixture in aqueous dispersion) in comparison to pure Ag NP. To identify a possible sacrificial anode effect (enhanced Ag^+ release) induced by the physical mixture, we analyzed the antimicrobial activity towards gram-positive *Staphylococcus aureus* (*S. aureus*) and gram-negative *Escherichia coli* (*E. coli*) as well as the viability of human mesenchymal stem cells (hMSC). In addition, ultraviolet–visible (UV-Vis) spectroscopy, cyclic voltammetry (CV), and atomic absorption spectroscopy (AAS) were performed to assess the Ag NP dissolution.

2. Materials and Methods

2.1 Nanoparticles

Pure Ag NP and pure Pt NP were synthesized as reported earlier [22] by reducing silver nitrate ($AgNO_3$; >99.9%, Carl Roth, Karlsruhe, Germany) or hexachloroplatinic acid (H_2PtCl_6; >99.9%, Carl Roth) with sodium borohydride ($NaBH_4$; ≥96%, Sigma-Aldrich, Taufkirchen, Germany) or citrate/tannic acid (anhydrous 98%, Acros *Organics*™, Nidderau, Germany / Fluka, Munich, Germany). The NP were coated with poly(N-vinylpyrrolidone) (PVP, Povidon 30, M = 40,000 g mol^{-1}, Fluka), and the average NP diameter was about 7 nm for both NP species, as was analyzed by differential centrifugal sedimentation (DCS) and high resolution transmission electron microscopy (HR-TEM) [22]. For full characterization data of Ag NP and Pt NP see Rostek *et al.*, 2018 [22].

The synthesized NP were stored in degassed ultrapure water under argon until further analysis or application. Stock solutions of NP were prepared in sterile ultrapure water (1.0, 0.7, 0.5, 0.2, 0.1 mg mL^{-1}). To achieve the final metal concentrations of 50, 35, 25, 10 and 5 µg mL^{-1} of each dispersion 50 µL were added per 1 mL of sample. Physical mixtures of Ag NP and Pt NP were prepared by simply mixing of the two monometallic NP dispersions.

Solutions of silver acetate (AgAc; ReagentPlus 99%, Sigma-Aldrich) used as Ag^+ control were prepared in sterile ultrapure water and normalized to the total content of Ag.

2.2 Microbiology

Escherichia coli DH5a (*E. coli*; German Collection of Microorganisms and Cell Cultures (DSMZ) 6897) and *Staphylococcus aureus* (*S. aureus*; DSMZ 1104) were cultured overnight in RPMI1640 (RPMI; GIBCO, Invitrogen, Karlsruhe, Germany) containing 10% (v/v) fetal calf serum (FCS; GIBCO, Invitrogen) and L-glutamine (0.3 g L^{-1}; GIBCO, Invitrogen) at 37 °C using a shaking water bath. Bacterial cell number was measured using a Densichek® turbidity photometer (bioMerieux, Lyon, France), based on turbidity standard solutions (McFarland scale).

The antimicrobial activity of NP was analyzed by determination of the minimum inhibitory concentration (MIC, lowest NP concentration able to inhibit bacterial growth) and the minimum bactericidal concentration (MBC, lowest NP concentration that kills 99.9% of the bacteria). Bacterial cell cultures were prepared by dilution of overnight cultures in RPMI/FCS. After addition of the different NP (35, 25, 10, 5 µg mL^{-1}), bacterial suspensions (10^5, 10^4, 10^3 colony forming units (CFU) mL^{-1}) were incubated for 24 h under cell culture conditions. Subsequently, the MIC was determined by visual assessment of the sample turbidity. The MBC was determined by plating of 50 µL of the samples without visible turbidity on Columbia agar plates (bioMerieux) and examination of the formed bacterial colonies after 24 h incubation at 37 °C in a microbial incubator.

2.3 Cell culture

Human mesenchymal stem cells (hMSC; 5^{th} to 10^{th} passage, Lonza, Basel, Switzerland) were cultivated in cell culture medium RPMI/FCS using 75 cm^2 culture flasks (BD Falcon, Becton Dickinson GmbH, Heidelberg, Germany). Cells were grown at 37 °C in a humidified 5% CO_2 atmosphere and sub-cultivated every 7 d to 14 d depending on cell proliferation.

Adherent subconfluently growing hMSC were detached from the culture flasks after washing with phosphate-buffered saline solution (PBS; GIBCO, Invitrogen) by addition of 0.2 mL cm^{-2} 0.25% trypsin/0.05% ethylenediaminetetraacetic acid (v/v) (EDTA, Sigma-Aldrich) for 5 min at 37 °C. Subsequently, cells were harvested, washed twice with RPMI/FCS and seeded at a density of 1.5 x 10^4 cells per well in 24-well cell culture plates (BD Falcon).

2.4 Cell viability

Adherent hMSC were treated either with dispersions of pure Ag NP, pure Pt NP or a physical mixture of Ag NP and Pt NP for 24 h in RPMI/FCS under cell culture conditions.

After NP exposure, cells were stained with 1 µM calcein-acetoxymethylester (calcein-AM; Calbiochem, Schwalbach, Germany) for 30 min at 37 °C and 50 µg mL^{-1} propidium iodide (PI; Sigma-Aldrich) for 10 min at RT (Live-Dead staining). Subsequently, the stained cells were analyzed by fluorescence microscopy (Olympus MVX10, Olympus, Hamburg, Germany). Cell viability was quantified by phase analysis (CellSens Dimensions, Olympus) calculating the calcein-fluorescent area. The data of NP treated hMSC was given as percentage of the non-treated control area, which was set as 100%.

Time-lapse microscopy was performed using the CytoSMART system (Lonza). Adherent hMSC were exposed to pure Ag NP (35 µg mL^{-1}), a physical mixture of Ag NP with Pt NP (35 µg mL^{-1} of each NP) or an AgAc solution (3.5 µg mL^{-1} Ag; Sigma-Aldrich) in RPMI/FCS under cell culture conditions and images of the cell culture were taken every 30 min.

2.5 Spectroscopic analysis

UV-Vis absorption spectra were recorded at room temperature using the UV-Vis spectrophotometer UVmini-1240 (Shimadzu, Kyōto, Japan) with semi-micro UV-cuvettes (Brandt GmbH, Wertheim, Germany).

Pure Ag NP (50 µg mL^{-1}) or a physical mixture of Ag NP with Pt NP (50 µg mL^{-1} of each NP) were dispersed in 1 mL cell culture medium RPMI. Absorption spectra between 300 nm and 500 nm were recorded directly after mixing of the NP (0 min) as well as after 5 min and 15 min incubation of the mixture at room temperature.

2.6 Cyclic voltammetry

For cyclic voltammetry (CV) measurements, a custom-made glassy carbon (GC) electrode (4 mm diameter) was used as the working electrode (WE). An Ag/AgCl, (3 M KCl (aq)) electrode was used as the reference electrode (RE; E = 207 mV vs. standard hydrogen electrode (SHE); SI analytics GmbH, Mainz, Germany). All potentials are given against this reference potential. A graphite rod (6 mm diameter) was used as counter electrode (CE). Before each experiment, the WE was polished to a mirror finish with 1 µm, 0.3 µm and 0.05 µm Al_2O_3 particle suspensions (LECO

Instruments GmbH). Afterwards, the GC electrode was cleaned by ultra-sonication for 3 min (Elmasonic S 100H, Singen, Germany).

NP dispersions of 1 mg mL^{-1} were then drop-cast onto the WE and dried in an argon flow. Pure Ag NP were applied as a single 2 µL drop. To achieve a physical mixture, Ag NP and Pt NP were simultaneously co-dropped (2 µL of each NP) on the WE. CV measurements were performed in a 0.1 M HCl (aq) solution with a scan rate of 100 mV s^{-1} between -0.2 V and 1.25 V. All measurements were carried out with an AutoLab PGStat-12 potentiostat (Metrohm, Herisan, Switzerland).

2.7 Dissolution experiments

Pure Ag NP (50 µg mL^{-1}) or a physical mixture of Ag NP with Pt NP (50 µg mL^{-1} of each NP) were incubated in 5 mL RPMI in the upper part of an Amicon Ultra-15 centrifugal filter (MWCO = 3,000 Da; Merck Chemicals GmbH, Darmstadt, Germany). After 60 min, 120 min and 180 min of incubation, the NP were separated from the released ions by centrifugation at 4,000 rpm for 60 min.

The remaining filtrate (500 µL) was subsequently mixed with 100 µL of concentrated nitric acid for Ag oxidation, and the Ag content was determined by atomic absorption spectrometry (AAS). AAS was carried out with a Thermo Electron M-Series instrument (Thermo Fisher Scientific, Waltham, USA) according to DIN EN ISO/IEC 17025:2005.

2.8 Statistical analysis

Data are expressed as mean ± standard deviation (SD) of at least three independent experiments. Statistical evaluation was performed by one-way analysis of variance (ANOVA) with Holm-Sidak-Test using SigmaPlot Software (Systat Software, Inc., CA, USA). p-Values less than 0.05 were considered as statistically significant.

3. Results

The postulated sacrificial anode effect and the resulting faster Ag^+ release from Ag NP induced by the presence of Pt NP was investigated by analysis of antimicrobial activity and cell viability as well as by UV-Vis, CV and AAS measurements of the physical mixture in comparison to a dispersion of pure Ag NP.

Three different physical mixtures were prepared containing 30 wt% Ag NP / 70 wt% Pt NP (Ag30/Pt70), 50 wt% Ag NP / 50 wt% Pt NP (Ag50/Pt50) and 70 wt% Ag NP / 30 wt% Pt NP (Ag70/Pt30). For comparison of the effects of pure Ag NP and the individual physical mixtures, the respective Ag NP concentration was kept constant, while the Pt NP concentration was varied.

3.1 Antimicrobial activity

Antimicrobial effects of physical mixtures containing Ag NP and Pt NP towards *S. aureus* and *E. coli* were analyzed in comparison to pure Ag NP and pure Pt NP. The Tables 1 and 2 summarize the resulting MBC values for *S. aureus* and *E. coli*, respectively.

Pure Pt NP showed no antimicrobial activity against *S. aureus* and *E. coli* even at the highest tested NP concentration of 35 µg mL^{-1}. In contrast, pure Ag NP exhibited significant antimicrobial effects on both strains. The antimicrobial activity of the physical mixtures Ag30/Pt70 and Ag50/Pt50 against *S. aureus* and *E. coli* was increased considerably compared to pure Ag NP, which is reflected by a decrease of the MBC values. However, the toxicity of the Ag70/Pt30 mixture was comparable to that of the pure Ag NP.

An inoculum effect (IE), which describes the decline of efficacy of antimicrobial agents at increasing bacterial cell number [23,24], was observed for pure Ag NP as well as for all physical mixtures and resulted in an increase of the MBC values for both strains (Tables 1 and 2). However, the overall toxicity ranking was not affected.

Table 1: MBC of pure Pt NP, pure Ag NP and the respective physical mixtures towards *S. aureus*, expressed in µg mL^{-1} of NP. For physical mixtures, the NP concentration refers to the Ag NP concentration. (>) indicates no bactericidal effect up to the given concentration, and (≥) indicates a bactericidal (MBC) effect at the given concentration and above.

S. aureus	10^5 CFU mL^{-1}	10^4 CFU mL^{-1}	10^3 CFU mL^{-1}
Pt NP **MBC** / µg mL^{-1}	> 35	> 35	> 35
Ag NP **MBC** / µg mL^{-1}	> 35	≥ 10 - 25	≥ 10
Ag30/Pt70 **MBC** / µg mL^{-1} Ag NP	≥ 10 - 25	≥ 10	≥ 5
Ag50/Pt50 **MBC** / µg mL^{-1} Ag NP	≥ 10 - 25	≥ 10	≥ 5
Ag70/Pt30 **MBC** / µg mL^{-1} Ag NP	≥ 25 - 35	≥ 10	≥ 10

Table 2: MBC of pure Pt NP, pure Ag NP and the respective physical mixtures towards *E. coli*, expressed in µg mL^{-1} of NP. For physical mixtures, the NP concentration refers to the Ag NP concentration. (>) indicates no bactericidal effect up to the given concentration and (≥) indicates a bactericidal (MBC) effect at the given concentration and above.

E. coli	10^5 CFU mL^{-1}	10^4 CFU mL^{-1}	10^3 CFU mL^{-1}
Pt NP **MBC** / µg mL^{-1}	> 35	> 35	> 35
Ag NP **MBC** / µg mL^{-1}	≥ 35	≥ 10 - 25	≥ 5
Ag30/Pt70 **MBC** / µg mL^{-1} Ag NP	≥ 10 - 25	≥ 5 - 10	≥ 5
Ag50/Pt50 **MBC** / µg mL^{-1} Ag NP	≥ 25 - 35	≥ 10	≥ 5
Ag70/Pt30 **MBC** / µg mL^{-1} Ag NP	≥ 35	≥ 10 - 25	≥ 5

3.2 Cell viability

As was previously reported, released Ag^+ exert cytotoxic effects on prokaryotic and eukaryotic cells at comparable concentrations [25]. Therefore, the influence of pure Ag NP, pure Pt NP and the respective physical mixtures on the viability of hMSC was analyzed by live-dead staining (Figure 1).

Pure Ag NP exhibited significant cell-toxic effects at a concentration of 25 µg mL^{-1} in comparison to the control (untreated hMSC) (Figure 1A - B), whereas Ag NP concentrations below 25 µg mL^{-1} had no adverse effect on cell viability (Figure 1C - D). By contrast, for the physical mixture Ag50/Pt50 cell toxicity was observed already at 10 µg mL^{-1} of Ag NP (Figure 1E - G).

The quantification of cell viability is summarized in Figure 2. Pure Ag NP led to a significant cell toxicity at Ag concentrations of 35 µg mL^{-1} and 25 µg mL^{-1}, while at 10 µg mL^{-1} no detectable cell toxicity occurred. Compared to pure Ag NP, the physical mixtures Ag30/Pt70 and Ag50/Pt50 led to significant cell toxic effects already at 10 µg mL^{-1} of Ag NP. In agreement with the antimicrobial activity results (section 3.1) a Pt NP content of 30 wt% in the physical mixture did not lead to higher toxicity in comparison to pure Ag NP. After 24 h of exposure no cell toxicity was observed for pure Pt NP up to an NP concentration of 35 µg mL^{-1}.

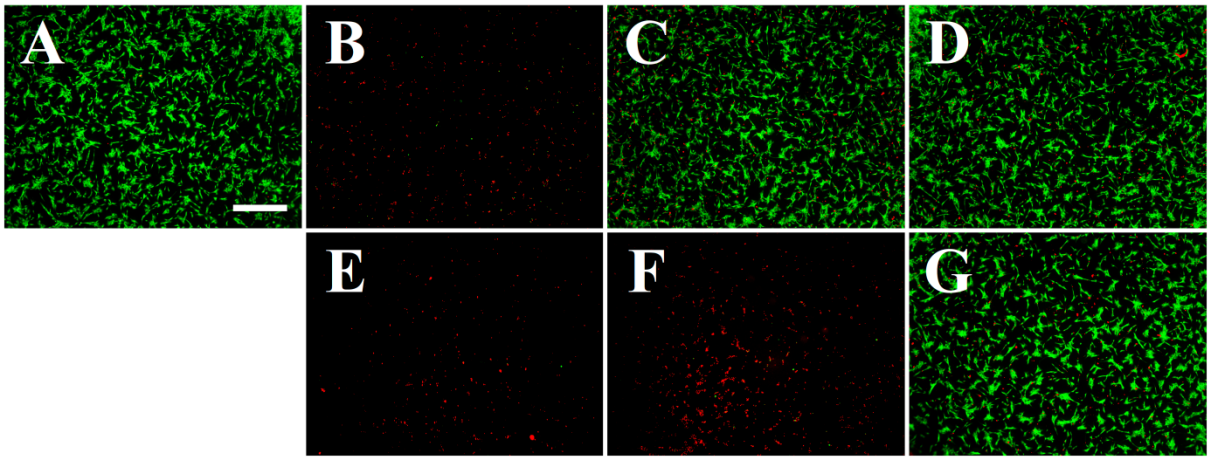

Figure 1: Cell viability of hMSC after NP exposure. Representative fluorescence images of hMSC incubated for 24 h with different NP in RMPI/FCS. Cells were stained with calcein-AM (green fluorescence) and PI (red fluorescence) to visualize the morphology of live and dead cells, respectively. **A:** hMSC control (no NP exposure). hMSC treated with pure Ag NP (**B:** 25 µg mL^{-1}, **C:** 10 µg mL^{-1}, **D:**

5 µg mL^{-1}) or the Ag50/Pt50 physical NP mixture (**E:** 25 µg mL^{-1} each, **F:** 10 µg mL^{-1}, **G:** 5 µg mL^{-1} of each NP). Scale bar = 2000 µm.

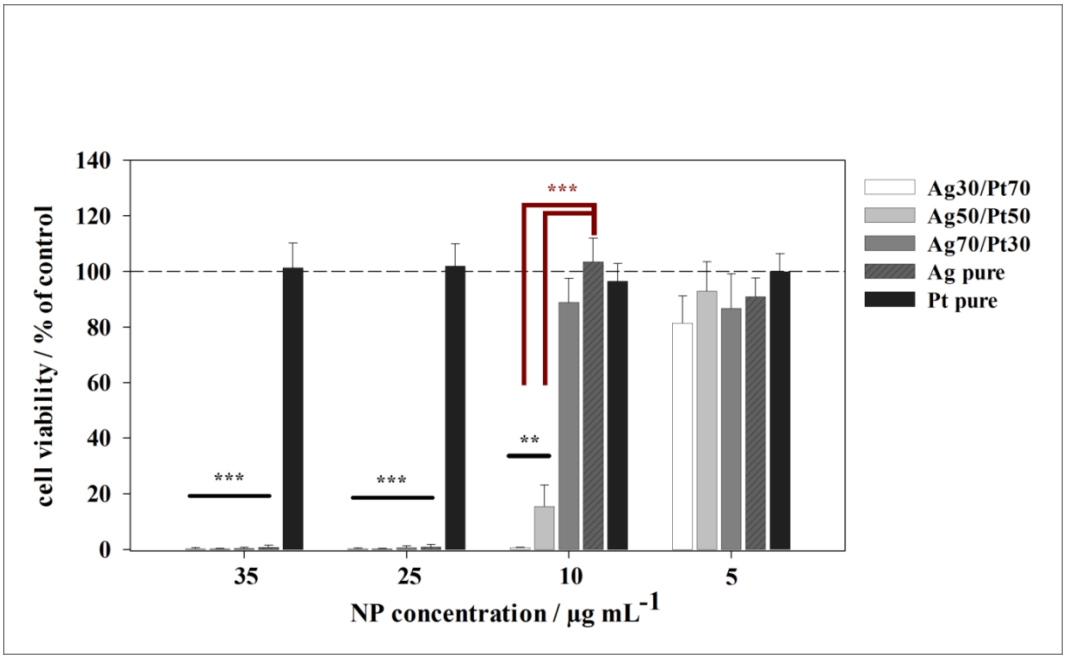

Figure 2: Quantification of cell viability of hMSC after NP exposure. hMSC were incubated for 24 h with different NP in RMPI/FCS. Cell viability was determined by phase analysis of the calcein-AM staining. For physical mixtures, the NP concentration refers to the Ag NP concentration. Data are expressed as mean ± SD of at least three independent experiments and given as the percentage of control (no NP exposure). Asterisks indicate significant differences (** $p \leq 0.01$, *** $p \leq 0.001$) in comparison to the control (black) or between pure Ag NP and the physical mixtures (red).

Time-lapse microscopy was used to elucidate whether the cell-toxic effects occurred faster with the physical mixtures than with pure Ag NP. Therefore, adherent hMSC were exposed to pure Ag NP, the physical mixture Ag50/Pt50 or an AgAc solution (Ag^+ control) in RPMI/FCS and images of the cell culture morphology were taken every 30 min.

As is shown in Figure 3 (row A), cells incubated with 35 µg mL^{-1} of pure Ag NP for 2 h were plastic-adherent and showed a typical fibroblast-like morphology similar to untreated hMSC. Hence, pure Ag NP induced no visible cell toxicity after 2 h of incubation. For the physical mixture Ag50/Pt50 containing the same concentration of Ag NP, toxic effects were observed already after 60 min of incubation, which was

visible by morphological changes of the cells (cells became spherical and detached from cell culture bottom; Figure 3, row B). After 90 min of incubation in the presence of the physical mixture, all cells had detached. Thus, the presence of Pt NP in the physical mixture with Ag NP caused a very fast cell death, comparable to the effect of the AgAc solution (solution of Ag^+) which led to complete cell detachment within 60 min of incubation (Figure 3, row C).

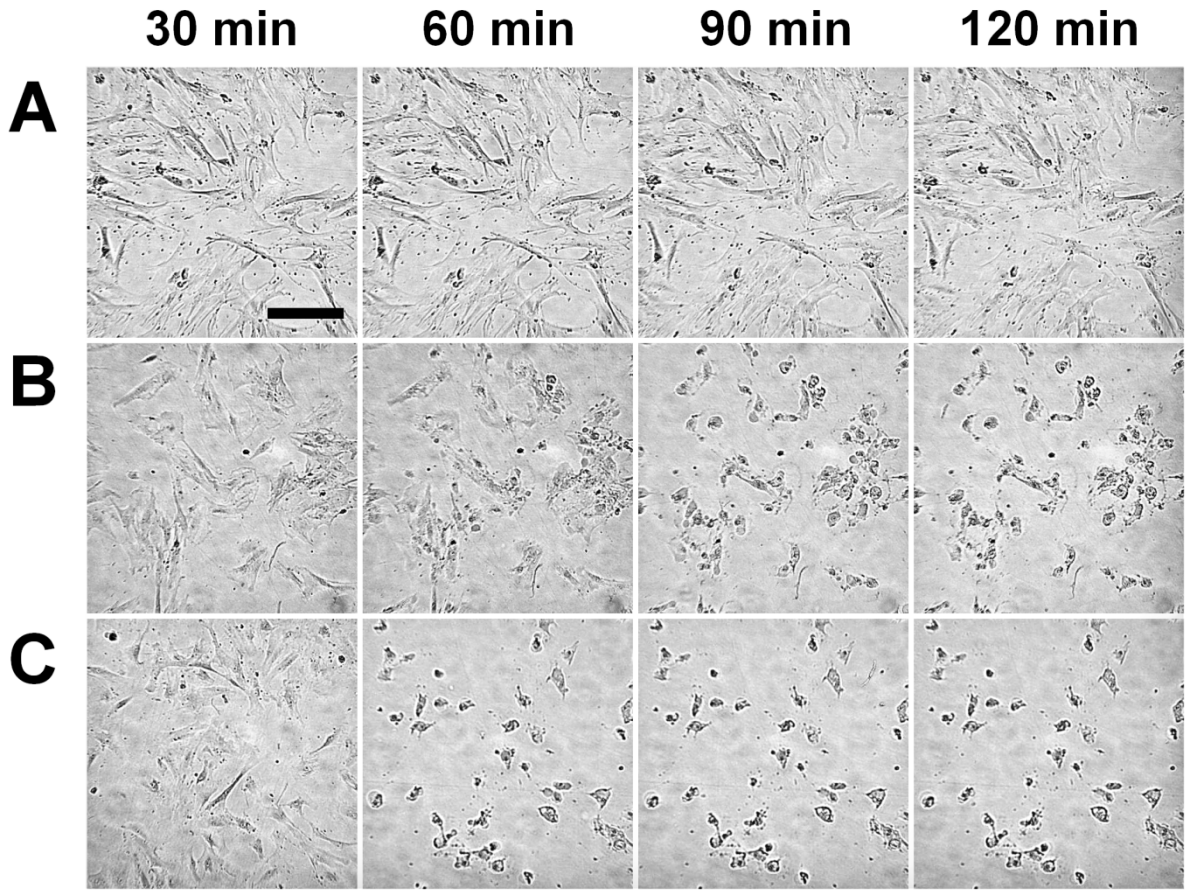

Figure 3: Time-lapse microscopy of hMSC during NP exposure. Representative time-lapse images of hMSC incubated with pure Ag NP (35 µg mL^{-1}, **row A**), the Ag50/Pt50 physical mixture (35 µg mL^{-1} of each NP, **row B**), and an AgAc solution (3.5 µg mL^{-1} Ag, **row C**). Living cells are plastic-adherent with a typical fibroblast-like morphology. Dead cells can be recognized by changed morphology (spherical, detaching cells). Scale bar = 200 µm.

3.3 Spectroscopic analysis

Dispersions of Ag NP exhibit a characteristic optical absorption spectrum due to surface plasmon resonance (SPR) which correlates with the particle morphology [26–

29]. Spherical and approximately spherical Ag NP display a single absorption maximum between 390 nm and 460 nm, depending on the particle size [26,30,31]. Therefore, changes in peak height, area and position can be used to monitor an altered particle size, shape or surface, e.g. by NP dissolution.

To track the time-dependent change of the Ag NP absorption spectra, pure Ag NP or the physical mixture Ag50/Pt50 were dispersed in RPMI and the spectra were measured between 300 nm and 500 nm. As is shown in Figure 4A, the Ag NP used in this study (spherical, diameter about 7 nm) displayed one single absorption maximum at 400 nm. Pure Pt NP does not have an absorption maximum in this wavelength range [32]. The height of the absorption peak of pure Ag NP decreased slightly during 15 min of incubation in RPMI, indicating a minor NP transformation (Figure 4A). In contrast, in the case of the physical mixture the plasmon Ag peak declined rapidly after 5 min of incubation in RPMI and disappeared completely already after 15 min of incubation in RPMI (Figure 4B). The fast and strong decline of the Ag NP absorption peak in the physical mixture suggests that a substantial Ag NP alteration has taken place.

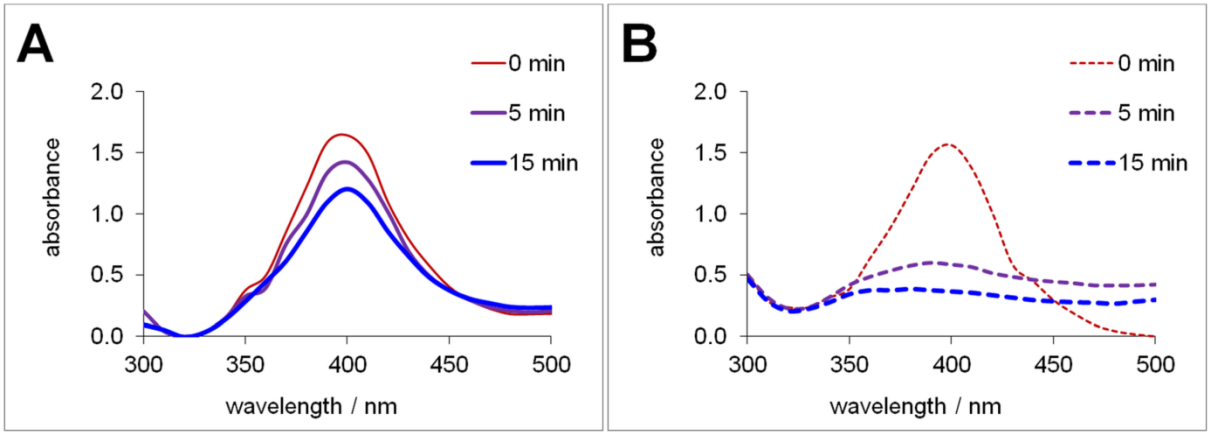

Figure 4: Time-resolved UV-Vis absorption spectra of **A:** pure Ag NP (50 µg mL^{-1}) in RPMI and **B:** the Ag50/Pt50 physical mixture (50 µg mL^{-1} of each NP) in RPMI. The peak at 400 nm corresponds to the surface plasmon resonance of Ag NP.

3.4 Cyclic voltammetry

The Ag^+ release within the Ag50/Pt50 physical mixture was investigated by CV analysis in comparison to pure Ag NP. The resulting cyclic voltammograms are shown in Figure 5.

Pure Ag NP displayed a large characteristic peak at about 0.2 V corresponding to the release of Ag^+ due to Ag oxidation and associated to the formation of silver chloride in chloride-containing solvents (here 0.1 M HCl (aq)). The reduction of Ag^+ to Ag occurred between 0.0 V and -0.2 V, which can be attributed to the reduction of the sparingly soluble silver chloride and is in accordance with published data [33,34]. For the physical NP mixture Ag50/Pt50 almost no signal for Ag oxidation and no Ag reduction signals were observed, which indicates an already completed Ag NP dissolution. Also no peak broadening and shifting to higher oxidation potentials (alloy signal) was observable, as reported for alloyed particles due to an electrochemical Ag stabilization [34,35].

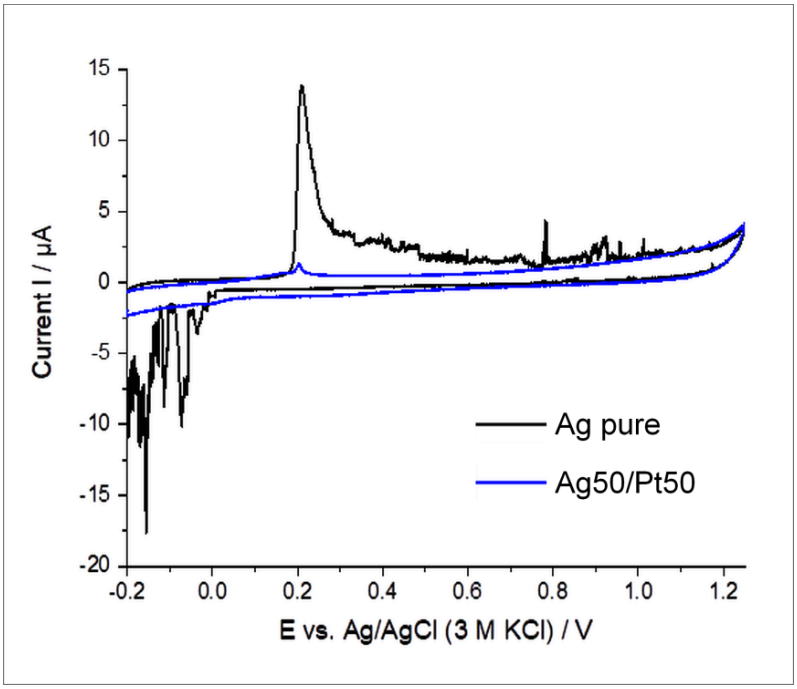

Figure 5: Cyclic voltammograms of pure Ag NP and the physical mixture Ag50/Pt50. NP dispersions (1 mg mL^{-1}) were drop-cast onto the WE (2 µL pure Ag NP or 2 µL Ag NP and 2 µL Pt NP) and dried in an argon flow. CV measurements were performed in a 0.1 M HCl (aq) solution with a scan rate of 100 mV s^{-1}.

3.5 Dissolution experiments

To prove whether the Ag^+ release from Ag NP was enhanced in the presence of Pt NP in the physical mixture compared to pure Ag NP, dissolution experiments in cell culture medium RPMI were performed and the Ag^+ release was analyzed by AAS.

As is shown in Figure 6, the amount of Ag^+ released from pure Ag NP after 180 min of incubation was about 1 wt% of the total Ag NP mass. For the physical Ag50/Pt50 mixture (containing same total Ag NP mass) 1 wt% Ag^+ was released already after 60 min of incubation and increased to 4 wt% Ag^+ after 180 min of incubation (Figure 6). Hence, the quantity of released Ag^+ from Ag NP was four times enhanced when Pt NP were present.

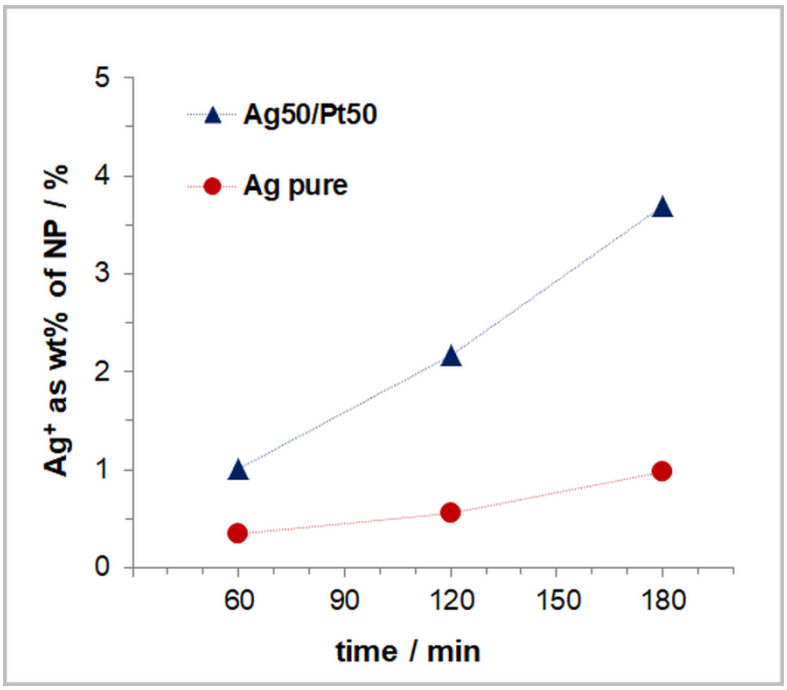

Figure 6: Release of Ag^+ as a function of time. Pure Ag NP (50 µg mL^{-1}) or a physical Ag50/Pt50 mixture (50 µg mL^{-1} of each NP) were incubated for 60 min, 120 min and 180 min in RPMI. The released Ag^+ was determined by AAS and is given as wt% of the total Ag NP mass applied.

4. Discussion

Here we have demonstrated that a higher Ag^+ release due to a faster Ag NP dissolution occurred when Pt NP were mixed with Ag NP (physical mixture) compared to same amounts of pure Ag NP. This effect was obviously electrochemically driven by a sacrificial anode reaction, considering the applied cell biological and analytical examination (toxic effects on bacteria and hMSC, UV-Vis, CV, AAS).

The enhanced Ag^+ release within the physical mixture was dependent on the ratio of Ag NP and Pt NP. A significant increase in cytotoxic reactions of the physical mixtures was observed with 50 wt% as well as 70 wt% Pt NP, while a Pt NP content of 30 wt% was insufficient to provoke enhanced toxicity. To the best of our knowledge, such a Pt-dependent enhancement of Ag dissolution has not yet been described for NP mixtures. There are only few studies that have addressed biological effects of sacrificial anode-like systems consisting of Ag and Pt. Dowling *et al.* and Zhang *et al.* demonstrated increased antimicrobial activity of bimetallic AgPt coatings compared to pure Ag due to an enhanced Ag^+ release [18,19]. The utilization of Ag dot arrays on Pt thin films as a sacrificial anode system was previously reported by our group and its efficiency to combat adherent and planctonic bacteria was confirmed [13].

Time-lapse microscopy and dissolution experiments demonstrated a fast Ag^+ release within the physical mixture. This is probably the reason for the electrochemical results obtained by cyclic voltammetry. The cyclovoltammogram recorded for the physical mixture showed an already completed Ag^+ release (no Ag oxidation and no Ag reduction signals) in contrast to the behavior of pure Ag NP, obviously due to the experimental setup, which required a droplet-drying phase before measurement.

Recently, we reported that bimetallic AgPt NP with an alloy-like structure (diameter about 10 nm) did not show any sacrificial anode effect for Ag [20,21], which is apparently a consequence of an increase in the redox potential of Ag in a Pt alloy. Such an electrochemical stabilization of Ag was also described for bimetallic alloyed AgAu NP [34–36]. The absence of a sacrificial anode effect in alloyed systems suggests that a sufficient physical separation of the metals is necessary to induce sacrificial anode effects. For most practical applications of sacrificial anode systems (e.g corrosion protection), there is such a physical separation of the bulk material, but the materials are in electrical contact [15]. A physical NP mixture is different in terms of the contact between the metals. A NP within a physical mixture interacts with others by collision due to random motion of the NP in suspension (convection and Brownian motion). The fact that the plasmon resonance of the Ag NP rapidly decreased in the presence of Pt NP suggests that the interaction of both particle types led to a morphological alteration of the Ag NP [26,30,31,37].

As was reported by Toshima *et al.* and Hirakawa *et al.,* physical mixtures of Ag NP (diameter about 10 nm) and more noble metal NP (platinum, palladium, rhodium;

diameter 2 - 3 nm) led to a spontaneous formation of bimetallic core/shell structured NP, consisting of an Ag core with a shell of the more noble metal [32,38–42]. They also observed a fast decline of the Ag plasmon peak in the respective physical mixtures, which was related to the coverage of the Ag NP surface with the more noble NP. Although the authors did not consider the electrochemical dissolution of Ag NP, they reported that the emerging bimetallic NP were smaller than the original Ag NP, which suggests that at least a partial dissolution of Ag NP occurred.

Currently, we cannot exclude that such a clustering of Ag NP and Pt NP occurred in our experimental physical mixtures, therefore the detailed mechanism of Ag^+ release enhancement within the studied physical mixtures still needs to be investigated in detail. Nevertheless, we suggest an underlying sacrificial anode mechanism which results in an enhanced Ag^+ release.

Very recently we reported that small Pt NP (as used in this study) exhibit an osteo-promotive activity on hMSC [21]. Therefore, physical mixtures of Ag NP and Pt NP could be useful for the development of novel biomaterials with enhanced antimicrobial activity and osteo-supportive properties at a reduced silver content, thereby reducing the inherent toxicity to the surrounding tissue.

Declarations of interest

None.

Acknowledgement

Supported by the Deutsche Forschungsgemeinschaft (DFG) in the projects EP 22/44-1, SE 2449/2-1, and HE 7192/2-1. We thank Kerstin Brauner and Robin Meya for AAS measurements.

References

[1] C.L. Romanò, M. Toscano, D. Romanò, L. Drago, Antibiofilm agents and implant-related infections in orthopaedics: Where are we? J. Chemother. 25 (2) (2013) 67–80. https://doi.org/10.1179/1973947812Y.0000000045.

[2] V. Alt, T. Bechert, P. Steinrücke, M. Wagener, P. Seidel, E. Dingeldein, E. Domann, R. Schnettler, An in vitro assessment of the antibacterial properties and cytotoxicity of nanoparticulate silver bone cement, Biomaterials 25 (18) (2004) 4383–4391. https://doi.org/10.1016/j.biomaterials.2003.10.078.

[3] B. Nowack, H.F. Krug, M. Height, 120 years of nanosilver history: Implications for policy makers, Environ. Sci. Technol. 45 (4) (2011) 1177–1183. https://doi.org/10.1021/es103316q.

[4] Q.L. Feng, J. Wu, G.Q. Chen, F.Z. Cui, T.N. Kim, J.O. Kim, A mechanistic study of the antibacterial effect of silver ions on Escherichia coli and Staphylococcus aureus, J. Biomed. Mater. Res. 52 (4) (2000) 662–668. https://doi.org/10.1002/1097-4636(20001215)52:4<662:AID-JBM10>3.0.CO;2-3.

[5] C.H. Ho, E.K. Odermatt, I. Berndt, J.C. Tiller, Long-term active antimicrobial coatings for surgical sutures based on silver nanoparticles and hyperbranched polylysine, J. Biomater. Sci. Polym. Ed. 24 (13) (2013) 1589–1600. https://doi.org/10.1080/09205063.2013.782803.

[6] M.H. Kollef, B. Afessa, A. Anzueto, C. Veremakis, K.M. Kerr, B.D. Margolis, D.E. Craven, P.R. Roberts, A.C. Arroliga, R.D. Hubmayr, M.I. Restrepo, W.R. Auger, R. Schinner, Silver-coated endotracheal tubes and incidence of ventilator-associated pneumonia: The NASCENT randomized trial, JAMA 300 (7) (2008) 805–813. https://doi.org/10.1001/jama.300.7.805.

[7] R. Vazquez-Muñoz, B. Borrego, K. Juárez-Moreno, M. García-García, J.D. Mota Morales, N. Bogdanchikova, A. Huerta-Saquero, Toxicity of silver nanoparticles in biological systems: Does the complexity of biological systems matter? Toxicol. Lett. 276 (2017) 11–20. https://doi.org/10.1016/j.toxlet.2017.05.007.

[8] S. Ahlberg, A. Antonopulos, J. Diendorf, R. Dringen, M. Epple, R. Flöck, W. Goedecke, C. Graf, N. Haberl, J. Helmlinger, F. Herzog, F. Heuer, S. Hirn, C. Johannes, S. Kittler, M. Köller, K. Korn, W.G. Kreyling, F. Krombach, J. Lademann, K. Loza, E.M. Luther, M. Malissek, M.C. Meinke, D. Nordmeyer, A. Pailliart, J. Raabe, F. Rancan, B. Rothen-Rutishauser, E. Rühl, C. Schleh, A.

Seibel, C. Sengstock, L. Treuel, A. Vogt, K. Weber, R. Zellner, PVP-coated, negatively charged silver nanoparticles: A multi-center study of their physicochemical characteristics, cell culture and in vivo experiments, Beilstein J. Nanotechnol. 5 (2014) 1944–1965. https://doi.org/10.3762/bjnano.5.205.

[9] M. Ahamed, M. Karns, M. Goodson, J. Rowe, S.M. Hussain, J.J. Schlager, Y. Hong, DNA damage response to different surface chemistry of silver nanoparticles in mammalian cells, Toxicol. Appl. Pharmacol. 233 (3) (2008) 404–410. https://doi.org/10.1016/j.taap.2008.09.015.

[10] K. Loza, J. Diendorf, C. Sengstock, L. Ruiz-Gonzalez, J.M. Gonzalez-Calbet, M. Vallet-Regi, M. Köller, M. Epple, The dissolution and biological effects of silver nanoparticles in biological media, J. Mater. Chem. B 2 (12) (2014) 1634. https://doi.org/10.1039/c3tb21569e.

[11] S. Chernousova, M. Epple, Silver as antibacterial agent: Ion, nanoparticle, and metal, Angew. Chem. Int. Ed Engl. 52 (6) (2013) 1636–1653. https://doi.org/10.1002/anie.201205923.

[12] M. Köller, C. Sengstock, Y. Motemani, C. Khare, P.J.S. Buenconsejo, J. Geukes, T.A. Schildhauer, A. Ludwig, Antibacterial activity of microstructured Ag/Au sacrificial anode thin films, Mater. Sci. Eng. C Mater. Biol. Appl. 46 (2015) 276–280. https://doi.org/10.1016/j.msec.2014.10.058.

[13] M. Köller, P. Bellova, S.M. Javid, Y. Motemani, C. Khare, C. Sengstock, K. Tschulik, T.A. Schildhauer, A. Ludwig, Antibacterial activity of microstructured sacrificial anode thin films by combination of silver with platinum group elements (platinum, palladium, iridium), Mater. Sci. Eng. C Mater. Biol. Appl. 74 (2017) 536–541. https://doi.org/10.1016/j.msec.2016.12.075.

[14] A. Abuayyash, N. Ziegler, J. Gessmann, C. Sengstock, T.A. Schildhauer, A. Ludwig, M. Köller, Antibacterial Efficacy of Sacrifical Anode Thin Films Combining Silver with Platinum Group Elements within a Bacteria-Containing Human Plasma Clot, Adv. Eng. Mater. 20 (2) (2018) 1700493. https://doi.org/10.1002/adem.201700493.

[15] S. Szabo, I. Bakos, Cathodic Protection with Sacrificial Anodes, Corrosion Reviews 24 (3-4) (2006) 18. https://doi.org/10.1515/CORRREV.2006.24.3-4.231.

[16] G.J. Bruce, D.J. Eyres (Eds.), Ship Construction, 7th ed., Elsevier; Butterworth-Heinemann, Amsterdam, Oxford, 2012.

[17] J. Chaussard, J.-C. Folest, J.-Y. Nedelec, J. Perichon, S. Sibille, M. Troupel, Use of Sacrificial Anodes in Electrochemical Functionalization of Organic Halides, Synthesis 1990 (05) (1990) 369–381. https://doi.org/10.1055/s-1990-26880.

[18] M. Zhang, Y. Zhao, L. Yan, R. Peltier, W. Hui, X. Yao, Y. Cui, X. Chen, H. Sun, Z. Wang, Interfacial Engineering of Bimetallic Ag/Pt Nanoparticles on Reduced Graphene Oxide Matrix for Enhanced Antimicrobial Activity, ACS Appl. Mater. Interfaces 8 (13) (2016) 8834–8840. https://doi.org/10.1021/acsami.6b01396.

[19] D.P. Dowling, A.J. Betts, C. Pope, M.L. McConnell, R. Eloy, M.N. Arnaud, Anti-bacterial silver coatings exhibiting enhanced activity through the addition of platinum, Surface and Coatings Technology 163-164 (2003) 637–640. https://doi.org/10.1016/S0257-8972(02)00689-8.

[20] V. Grasmik, M. Breisch, K. Loza, M. Heggen, M. Köller, C. Sengstock, M. Epple, Synthesis and biological characterization of alloyed silver–platinum nanoparticles: From compact core–shell nanoparticles to hollow nanoalloys, RSC Adv. 8 (67) (2018) 38582–38590. https://doi.org/10.1039/C8RA06461J.

[21] M. Breisch, V. Grasmik, K. Loza, K. Pappert, A. Rostek, N. Ziegler, A. Ludwig, M. Heggen, M. Epple, J.C. Tiller, T.A. Schildhauer, M. Köller, C. Sengstock, Bimetallic silver-platinum nanoparticles with combined osteo-promotive and antimicrobial activity, Nanotechnology 30 (30) (2019) 305101. https://doi.org/10.1088/1361-6528/ab172b.

[22] A. Rostek, M. Breisch, K. Pappert, K. Loza, M. Heggen, M. Köller, C. Sengstock, M. Epple, Comparative biological effects of spherical noble metal nanoparticles (Rh, Pd, Ag, Pt, Au) with 4–8 nm diameter, Beilstein J. Nanotechnol. 9 (2018) 2763–2774. https://doi.org/10.3762/bjnano.9.258.

[23] I. Brook, Inoculum Effect, Clinical Infectious Diseases 11 (3) (1989) 361–368. https://doi.org/10.1093/clinids/11.3.361.

[24] C. Tan, R.P. Smith, J.K. Srimani, K.A. Riccione, S. Prasada, M. Kuehn, L. You, The inoculum effect and band-pass bacterial response to periodic antibiotic treatment, Mol. Syst. Biol. 8 (2012) 617. https://doi.org/10.1038/msb.2012.49.

[25] C. Greulich, D. Braun, A. Peetsch, J. Diendorf, B. Siebers, M. Epple, M. Köller, The toxic effect of silver ions and silver nanoparticles towards bacteria and human cells occurs in the same concentration range, RSC Adv. 2 (17) (2012) 6981. https://doi.org/10.1039/c2ra20684f.

[26] S. Agnihotri, S. Mukherji, S. Mukherji, Size-controlled silver nanoparticles synthesized over the range 5–100 nm using the same protocol and their antibacterial efficacy, RSC Adv. 4 (8) (2014) 3974–3983. https://doi.org/10.1039/C3RA44507K.

[27] C. Noguez, Surface Plasmons on Metal Nanoparticles: The Influence of Shape and Physical Environment, J. Phys. Chem. C 111 (10) (2007) 3806–3819. https://doi.org/10.1021/jp066539m.

[28] A.L. González, C. Noguez, Influence of Morphology on the Optical Properties of Metal Nanoparticles, Jnl of Comp & Theo Nano 4 (2) (2007) 231–238. https://doi.org/10.1166/jctn.2007.2309.

[29] C. Chapon, M.F. Gillet, C.R. Henry (Eds.), Small Particles and Inorganic Clusters: Proceedings of the Fourth International Meeting on Small Particles and Inorganic Clusters University Aix-Marseille III Aix-en-Provence, France, 5-9 July 1988, Springer Berlin Heidelberg, Berlin, Heidelberg, 1989.

[30] R. Desai, V. Mankad, S. Gupta, P. Jha, Size Distribution of Silver Nanoparticles: UV-Visible Spectroscopic Assessment, nanosci nanotechnol lett 4 (1) (2012) 30–34. https://doi.org/10.1166/nnl.2012.1278.

[31] G. Mie, Contributions to the optics of turbid media particularly of colloidal metal solutions, Ann. Phys. 330 (3) (1908) 377–445. https://doi.org/10.1002/andp.19083300302.

[32] N. Toshima, M. Kanemaru, Y. Shiraishi, Y. Koga, Spontaneous formation of core/shell bimetallic nanoparticles: A calorimetric study, J. Phys. Chem. B 109 (34) (2005) 16326–16331. https://doi.org/10.1021/jp051400h.

[33] H.S. Toh, C. Batchelor-McAuley, K. Tschulik, R.G. Compton, Electrochemical detection of chloride levels in sweat using silver nanoparticles: A basis for the preliminary screening for cystic fibrosis, Analyst 138 (15) (2013) 4292–4297. https://doi.org/10.1039/C3AN00843F.

[34] E.N. Saw, V. Grasmik, C. Rurainsky, M. Epple, K. Tschulik, Electrochemistry at single bimetallic nanoparticles - using nano impacts for sizing and compositional analysis of individual AgAu alloy nanoparticles, Faraday Discuss. 193 (2016) 327–338. https://doi.org/10.1039/c6fd00112b.

[35] N. Alissawi, V. Zaporojtchenko, T. Strunskus, I. Kocabas, V.S.K. Chakravadhanula, L. Kienle, D. Garbe-Schönberg, F. Faupel, Effect of gold alloying on stability of silver nanoparticles and control of silver ion release from

vapor-deposited Ag–Au/polytetrafluoroethylene nanocomposites, Gold Bull 46 (1) (2013) 3–11. https://doi.org/10.1007/s13404-012-0073-6.

[36] V. Grasmik, C. Rurainsky, K. Loza, M.V. Evers, O. Prymak, M. Heggen, K. Tschulik, M. Epple, Deciphering the Surface Composition and the Internal Structure of Alloyed Silver-Gold Nanoparticles, Chemistry 24 (36) (2018) 9051–9060. https://doi.org/10.1002/chem.201800579.

[37] S.M. Oja, Y. Fan, C.M. Armstrong, P. Defnet, B. Zhang, Nanoscale Electrochemistry Revisited, Anal. Chem. 88 (1) (2016) 414–430. https://doi.org/10.1021/acs.analchem.5b04542.

[38] K. Hirakawa, Self-Organization of Silver-Core Bimetallic Nanoparticles and Their Application for Catalytic Reaction, in: A.A. Hashim (Ed.), Smart nanoparticles technology, InTech, Rijeka, Croatia, 2012. https://doi.org/10.5772/33918

[39] K. Hirakawa, N. Toshima, Ag/Rh Bimetallic Nanoparticles Formed by Self-assembly from Ag and Rh Monometallic Nanoparticles in Solution, Chem. Lett. 32 (1) (2003) 78–79. https://doi.org/10.1246/cl.2003.78.

[40] T. Matsushita, Y. Shiraishi, S. Horiuchi, N. Toshima, Synthesis and Catalysis of Polymer-Protected Pd/Ag/Rh Trimetallic Nanoparticles with a Core–Shell Structure, BCSJ 80 (6) (2007) 1217–1225. https://doi.org/10.1246/bcsj.80.1217.

[41] N. Toshima, Capped Bimetallic and Trimetallic Nanoparticles for Catalysis and Information Technology, Macromol. Symp. 270 (1) (2008) 27–39. https://doi.org/10.1002/masy.200851004.

[42] K. Hirakawa, T. Kaneko, N. Toshima, Kinetics of Spontaneous Bimetallization between Silver and Noble Metal Nanoparticles, Chemistry – An Asian Journal 13 (15) (2018) 1892–1896. https://doi.org/10.1002/asia.201800633.